nature materials

LETTERS

PUBLISHED ONLINE: 16 MARCH 2015 | DOI: 10.1038/NMAT4248

Design of compensated ferrimagnetic Heusler alloys for giant tunable exchange bias

Ajaya K. Nayak[1]*, Michael Nicklas[1], Stanislav Chadov[1], Panchanana Khuntia[1], Chandra Shekhar[1], Adel Kalache[1], Michael Baenitz[1], Yurii Skourski[2], Veerendra K. Guduru[3], Alessandro Puri[3], Uli Zeitler[3], J. M. D. Coey[4] and Claudia Felser[1]*

Rational material design can accelerate the discovery of materials with improved functionalities[1]. This approach can be implemented in Heusler compounds with tunable magnetic sublattices to demonstrate unprecedented magnetic properties[2]. Here, we have designed a family of Heusler alloys with a compensated ferrimagnetic state. In the vicinity of the compensation composition in Mn–Pt–Ga, a giant exchange bias (EB) of more than 3 T and a large coercivity are established. The large exchange anisotropy originates from the exchange interaction between the compensated host and ferrimagnetic clusters that arise from intrinsic anti-site disorder. Our design approach is also demonstrated on a second material with a magnetic transition above room temperature, Mn–Fe–Ga, exemplifying the universality of the concept and the feasibility of room-temperature applications. These findings may lead to the development of magneto-electronic devices and rare-earth-free exchange-biased hard magnets, where the second quadrant magnetization can be stabilized by the exchange bias.

Exchange bias produces a shift of the hysteresis loop of a ferromagnet along the magnetic field axis due to interfacial exchange coupling with an adjacent antiferromagnet[3,4]. It is employed for a variety of technological applications[3–10]. One of the most important uses of EB is in spin-valve devices, where an artificial antiferromagnet exchange biased by a normal antiferromagnet allows magnetoresistance to be developed in a small field, stabilizing the magnetic state against repeated cycling[9]. Although the origin of EB is still a subject of discussion, its phenomenology has variously been interpreted in terms of rough ferromagnetic (FM)–antiferromagnetic (AFM) interfaces[11,12], a domain-state model[13] and uncompensated interfacial spins[14,15]. Despite both FM and AFM subsystems being inseparable parts of an EB system, it is the latter that determines the magnitude of the bias in the system[15–17]. Therefore, it is important to search for an appropriate magnetically compensated material to observe a maximum effect. Besides the EB phenomenon, magnetically compensated materials are proposed to play a vital role in antiferromagnetic spintronics[18,19] and all-optical switching devices[20]. Single spin superconductivity has even been predicted in a spin-compensated half-metal[21]. In this letter we present a design scheme for a magnetically compensated ferrimagnet and demonstrate the relevance of this compensated magnetic state in realizing giant exchange bias and large coercivity.

Heusler compounds, which provide the material-base for our design scheme, are well known for their multi-functional properties[22–24]. The story of their success is based on the fact that new materials can be designed in the flexible structure of the Heusler family on the basis of simple rules taking into account the position of the atoms, the number of valence electrons, the degree of atomic disorder and the strength of the exchange interactions[2]. One of the famous examples of valence electron count is the robustness of the Slater–Pauling rule, connected to half-metallicity, in the $L2_1$ cubic Heusler compounds[25]. Together with the fact that in Heusler compounds Mn develops a strong localized magnetic moment, it can be used as a guide to search for compensated ferrimagnets in the Heusler family with 24 valence electrons. On the other hand, this provides us only a preliminary guide. The classical example is Mn_3Ga (ref. 26), which is predicted to exhibit a half-metallic state in the $L2_1$ cubic phase; but the cubic phase does not form in the bulk owing to electronic instability leading to a tetragonal strain breaking both the compensated and half-metallic states. A half-metallic compensated state can be recovered by chemical substitution[27]. Here, we focus on the compensated magnetic state.

Combining Mn_3Ga with another material of opposite net magnetization, Mn_2PtGa, forms an excellent starting point to design a zero-magnetization structure based on a compensated ferrimagnetic state. Mn_2PtGa consists of two non-equivalent types of Mn, one in the Mn–Ga and another in the Mn–Pt planes of the inverse tetragonal structure[28]. The Mn sitting in the Mn–Ga planes possesses a higher magnetic moment owing to its more localized nature. It couples antiferromagnetically to the Mn in the Mn–Pt planes. This configuration results in a net uncompensated magnetization of about 0.5 μ_B/f.u. arising from the larger moment of the Mn in the Mn–Ga planes (Fig. 1). On the other hand, the complete replacement of Pt by Mn to form Mn_3Ga results in one Mn in the Mn–Ga and two Mn in the Mn–Mn planes (former Mn–Pt plane). Thus, Mn_3Ga exhibits a net uncompensated magnetization of about 1 μ_B/f.u. of opposite sign to that in Mn_2PtGa (refs 26,29). This suggests that we can create a fully compensated magnet with a compensation point for a particular Mn/Pt ratio. The design scheme is depicted in Fig. 1. From first-principles calculations, it follows that the critical composition with zero magnetization is achieved in $Mn_{3-x}Pt_xGa$ at a Pt content of about $x_0 = 0.59$, which is in good agreement with the experimental findings. On optimizing the Mn/Pt ratio, we always find a small lack of compensation in the

[1]Max Planck Institute for Chemical Physics of Solids, Nöthnitzer Str. 40, D-01187 Dresden, Germany. [2]Dresden High Magnetic Field Laboratory (HLD-EMFL), Helmholtz-Zentrum Dresden-Rossendorf, D-01328 Dresden, Germany. [3]High Field Magnet Laboratory (HFML-EMFL), Radboud University, Toernooiveld 7, 6525 ED Nijmegen, The Netherlands. [4]School of Physics and CRANN, Trinity College, Dublin 2, Ireland.
*e-mail: nayak@cpfs.mpg.de; felser@cpfs.mpg.de

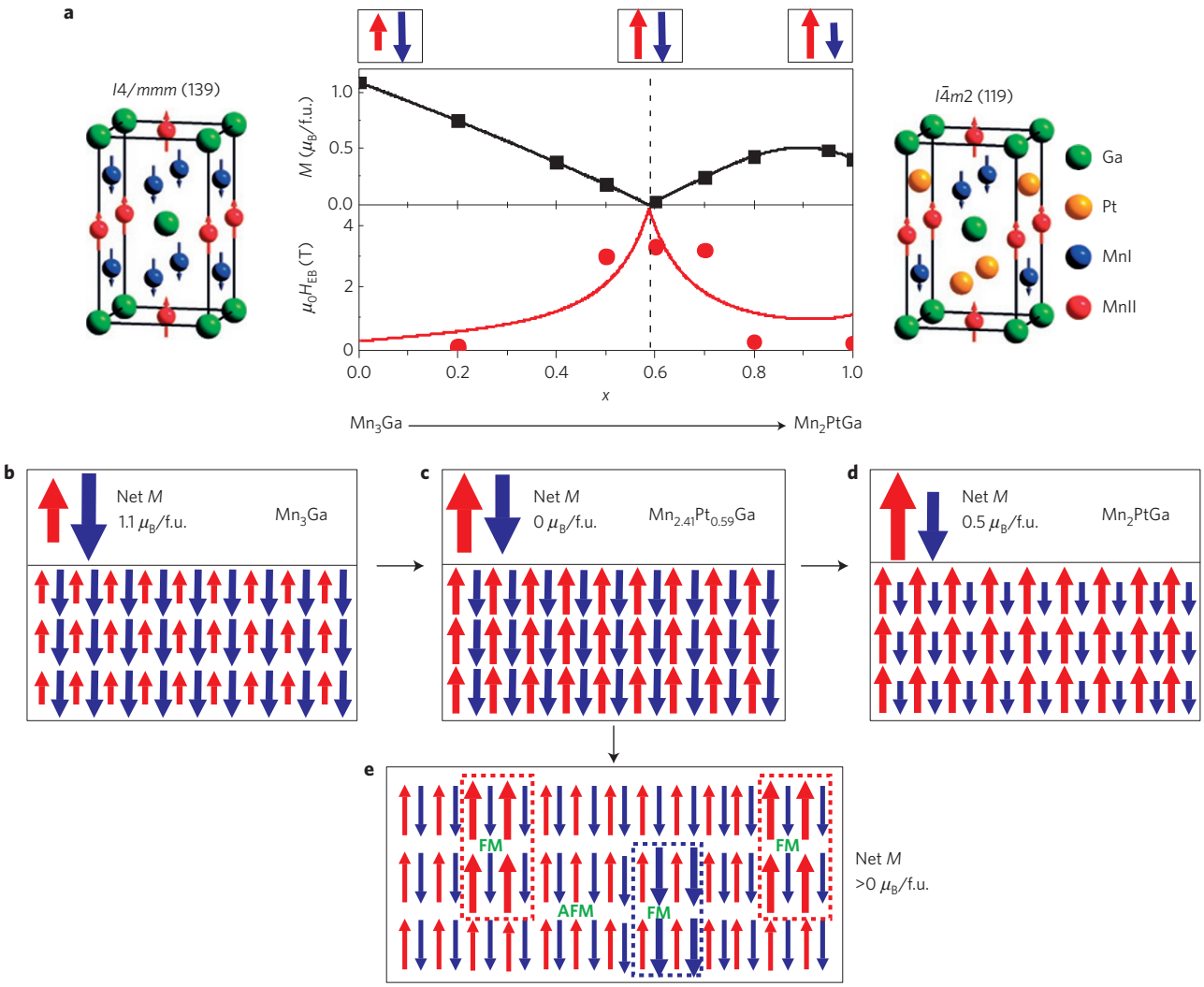

Figure 1 | Design of a compensated magnetic state. a, Uncompensated magnetization, M, in $Mn_{3-x}Pt_xGa$ going through a compensation point ($M=0$) at $x=0.59$ (upper panel): squares are results from theoretical calculations. The line is a guide to eye. Lower panel: Experimental EB field H_{EB} at 4.2 K (solid circles). The solid line corresponds to the result of our calculation. The regular and inverse Heusler structures of the Mn_3Ga and Mn_2PtGa are shown to the left and right respectively. **b**–**d**, Magnetic moments of Mn in two different sublattices for Mn_3Ga, $Mn_{2.41}Pt_{0.59}Ga$ and Mn_2PtGa. Red arrows correspond to Mn in the Mn–Ga plane and blue arrows to Mn in the Mn–Mn planes. The size and direction of the moment is indicated by the arrow. Perfect magnetic compensation is expected in $Mn_{2.41}Pt_{0.59}Ga$. **e**, FM domains (boundaries indicated by dashed lines) inside the compensated AFM host.

material due to anti-site disorder. This leads to an exceptionally large bulk EB and a large coercivity. In contrast to an artificial antiferromagnet, which is a thin-film structure composed of two ferromagnetic layers separated by a coupling layer[9], here we combine two isostructural ferrimagnetic compounds, Mn_3Ga and Mn_2PtGa, to obtain an intrinsically anisotropic compensated magnetic state on an atomic scale in the bulk.

To characterize the magnetic properties of $Mn_{3-x}Pt_xGa$ we have measured the temperature dependence of the magnetization, $M(T)$. We find a systematic increase in the Néel temperature (T_N) with increasing Mn content, as shown in Fig. 2. The irreversibility between the zero-field-cooled (ZFC) and field-cooled (FC) curves reflects the appearance of coercivity. We suggest that FM clusters embedded in the compensated host are the source of this irreversibility. NMR measurements confirm that these clusters originate from random interchange between Pt in the Mn–Pt planes and Mn in the Mn–Ga planes (Supplementary Information). The irreversibility between ZFC and FC $M(T)$ curves increases with increasing field, demonstrating that cooling in higher fields helps the FM clusters to grow in size (Supplementary Information).

The ZFC magnetization at 5 K shows an unsaturated behaviour for magnetic fields up to 14 T (inset of Fig. 2); therefore, higher fields are required to gain a better understanding of the magnetic state. Pulsed-field magnetization measurements at 4.2 K up to 60 T are shown in Fig. 3a. For $x=0.5$, 0.6 and 0.7 the hysteresis loops close at a field of 35–40 T. The non-saturating magnetization up to 60 T reflects the strength of the dominant inter-sublattice Mn–Mn exchange in the polycrystalline compensated ferrimagnetic host. The hysteresis reveals that there is a FM component of 0.1–0.3 μ_B in the compensated host, which may be compared with its ferromagnetic collinear saturation of about 6 μ_B/f.u. We further obtain coercive fields of $\mu_0 H_C = 2.2$, 3.6 and 3.0 T at 4.2 K for $x=0.5$, 0.6 and 0.7, respectively. These values are comparable to the maximum H_C observed in rare-earth-based hard magnetic bulk materials. To investigate the exchange interaction between the FM clusters and AFM host, we have measured FC hysteresis loops. The FC hysteresis loops taken at 4.2 K in a d.c.-field of ± 32 T are depicted in Fig. 3b. The loops for $x=0.5$, 0.6 and 0.7 exhibit a large shift in the negative field direction, indicating the existence of a large unidirectional anisotropy and a large

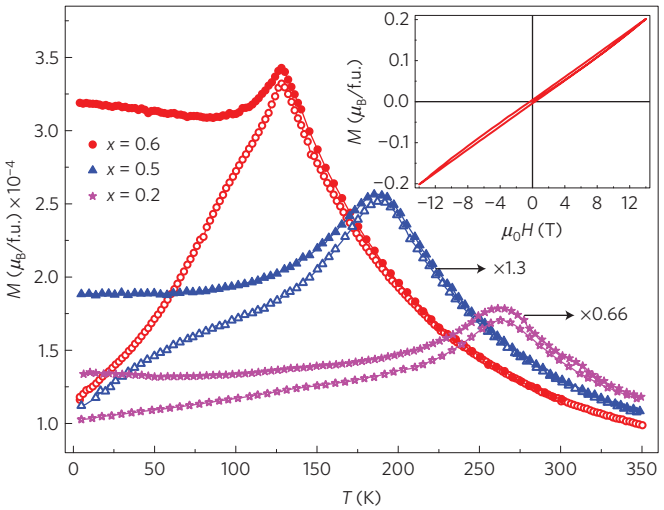

Figure 2 | Compensated ferrimagnetic state in Mn–Pt–Ga. $M(T)$ for $Mn_{3-x}Pt_xGa$ ($x=0.2$, 0.5 and 0.6) measured in a field of 0.01 T. Open symbols represent the zero-field-cooled (ZFC) curves and closed symbols the field-cooled (FC) curves. The lines are guides to the eye. In the ZFC mode, the sample was initially cooled to 2 K and the data were taken on increasing the temperature in an applied magnetic field. In the FC mode, the data were collected while decreasing the temperature in the presence of the field. The data for $x=0.2$ and $x=0.5$ have been multiplied by 0.66 and 1.3, respectively. The inset shows the zero-field-cooled $M(H)$ hysteresis loop for $Mn_{2.4}Pt_{0.6}Ga$ measured at 5 K in a field of ±14 T.

EB. All loops close in a field of 20–25 T. Interestingly, the FC hysteresis loops recorded after field cooling in 15 and 25 T follow a similar path. This implies that a cooling field of $\mu_0 H_{CF} = 15$ T is sufficient to saturate the FM moments and a larger cooling field does not further change the magnetic state (Fig. 3c). For all samples the FC $M(H)$ loops pass almost through the origin, resulting in nearly the same coercivity and EB. The EB increases monotonically for cooling fields up to 10 T and then saturates for higher fields.

In $Mn_{3-x}Pt_xGa$, we obtain a maximum conventional EB field of $H_{EB} = 3.3$ T for $x = 0.6$. This value is among the largest reported so far. We note that a small ZFC EB is observed only for samples very close to stoichiometric Mn_2PtGa. In particular we do not find a ZFC EB close to the compensation region. The dependence of the EB and coercivity on the Pt concentration measured after field cooling the sample in 15 T is shown in the inset of Fig. 4a. Both H_{EB} and the coercive field (H_C) exhibit a clear maximum around $x = 0.6$. We observe a small increase in H_C for FC loops in comparison to ZFC loops, as generally found for materials showing an EB effect[4,5,30]. The EB measured after field cooling in 5 T for $Mn_{2.4}Pt_{0.6}Ga$ and $Mn_{2.5}Pt_{0.5}Ga$ shows a monotonic decrease with increasing temperature and vanishes around T_N, as shown in Fig. 4a.

To establish a comprehensive picture we applied our design concept to another Heusler system in the Mn–Ga family, Mn–Fe–Ga, where the ordering temperature can be varied over a wide range to above room temperature by tuning the composition (Supplementary Figs 7–14). Furthermore, Mn_2FeGa is nearly in a compensated magnetic state, whereas Fe_2MnGa is ferromagnetic. By adjusting the composition we can achieve a material with ferromagnetic clusters in an almost compensated ferrimagnetic host and T_N above room temperature. Furthermore, these FM clusters can be established without Fe substitution by creating vacancies on the Mn location. The temperature dependence of the EB for $Mn_{1.5}Fe_{1.5}Ga$ and the sample with Mn vacancy, $Mn_{1.8}FeGa$, are shown in Fig. 4b. $Mn_{1.5}Fe_{1.5}Ga$ and $Mn_{1.8}FeGa$ exhibit an EB of 1.1 and 1.2 T at 2 K, respectively, which is observable up to room temperature.

Our experiments show that magnetic compensation of the host is an important requirement to achieve a large EB. We now introduce a model to explain these observations. Assuming ferromagnetic clusters in the compensated ferrimagnetic host that are coherent with the host and coupled to it via exchange bonds at the interface, we can elaborate the conditions for the EB. We assume that the FM clusters and their surroundings are part of a single-crystalline grain with a uniform orientation of the uniaxial magnetocrystalline anisotropy. By applying an external magnetic field which is large enough to rotate the magnetization in the ferromagnetic clusters, but small enough not to rotate the compensated ferrimagnetic host, we find (see Supplementary Equations 1–3) that the EB is described well by

$$H \approx \frac{12 J_{AB} S_A S_B (1-\cos(\theta_K-\theta_B)) \cdot L^2 n^{2/3} + K_B \sin^2(\theta_K-\theta_B) \cdot L^3 n}{\delta S_A \cdot \cos\theta_K \cdot N_A + S_B \cos\theta_B \cdot L^3 n} \quad (1)$$

where $S_{A(B)}$ are the amplitudes of the atomic magnetic moments in the host (cluster), δS_A accounts for the imperfect magnetic compensation in the host; N_A is the number of atoms inside the host; L is the linear size of the cluster, n is the atomic density; J_{AB} is the exchange coupling constant at the interface. $K_B > 0$ is the anisotropy constant for the cluster, $\theta_{K,B}$ are the polar angles referring to the orientation of the anisotropy axis and magnetization of the cluster, respectively.

In the case of small FM clusters ($L^3 n \ll N_A$) the key role is played by the compensation of the host. The EB field in equation (1) can be expressed as

$$H(M) \approx \frac{\alpha}{M+\beta} \quad (2)$$

where M is the total magnetization; α and β are parameters depending on the interface exchange coupling, the particular form of the interfaces, and the number, distribution and magnetic moments of the embedded ferromagnetic clusters. The theoretical estimate in equation (2) agrees well with experimental data that show a nearly inverse relationship between the H_{EB} and magnetization (Fig. 1a).

To estimate the maximum exchange-bias field equation (1) can be expressed in terms of the size of the ferromagnetic cluster (L),

$$H_{max}[\mathrm{T}] = 0.21 \times (1/L[\mathrm{Å}]) \times 10^5 + 0.54$$

where the first term appears from the interface exchange coupling and the second term from the magnetic anisotropy (Supplementary Information). To achieve the exchange-bias fields of 3 T, the characteristic FM cluster size must not exceed $L \sim 10^4$ Å.

A key experimental observation is that at low temperature the EB is almost equal to the coercivity in all samples. This can be explained by considering additional conditions for the magnetization switching. For simplicity, we consider only those grains which are oriented differently from the polar angle, $\theta_K = \pi/2$. Such grains exhibit a sharp rectangular-like hysteresis, in which the coercivity corresponds to a regime of fast domain-wall motion. This rapid process is the transition between two states: one state comprising the domain wall (induced by the competition between the strong negative magnetic field and the positive exchange pinning at the host/cluster interface) and another state which is magnetically

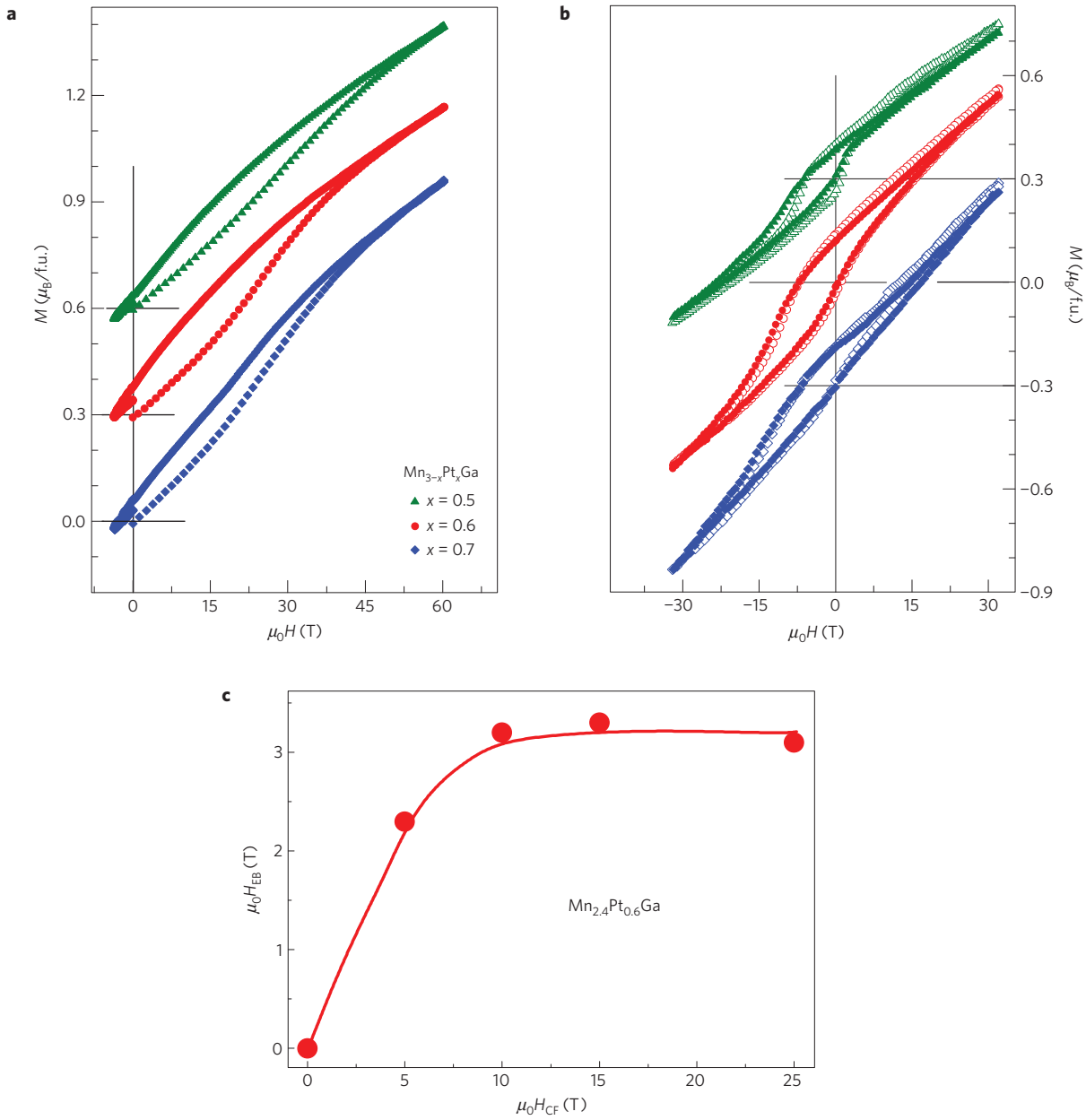

Figure 3 | Hysteresis loops in Mn–Pt–Ga. a, $M(H)$ isotherms measured up to 60 T at 4.2 K. The data for successive samples are shifted by 0.3 μ_B along the magnetization axis for better clarity. **b**, Field-cooled (FC) $M(H)$ loops measured up to ±32 T after field cooling the samples in $\mu_0 H_{CF} = 15$ T (closed symbols) and 25 T (open symbols). The loop for $x = 0.7$ is shifted by $-0.3\,\mu_B$ and for $x = 0.5$ by $+0.3\,\mu_B$ along the magnetization axis. The vertical and horizontal black lines represent the ordinate and the corresponding abscissa, respectively. **c**, The dependence of exchange-bias field (H_{EB}), red spheres, on the cooling field (H_{CF}). The red line is a guide to the eye. H_{EB} is calculated using $H_{EB} = -(H_C^+ + H_C^-)/2$, where H_C^+ and H_C^- are the lower and upper cutoff fields at which the magnetization becomes zero.

uniform. The elimination of the domain wall occurs for the small external field values ($H < 0$) at which the energies of these two states become comparable. The detailed theoretical interpretation can be found in Supplementary Information. From this model we estimate that H_C^+ is only about −1 mT, where the cluster size L is the leading contribution.

To conclude, we have established an approach to design compensated ferrimagnetic Heusler alloys. A small lack of compensation allows us to achieve an extremely large EB and matching coercivity. The present finding provides a new insight into the mechanism of EB and suggests exploring similar coherent materials that can be implemented in thin film form. Furthermore, the achievement of a coercivity of more than 3 T based on exchange anisotropy suggests a new approach to permanent magnet design, where the second quadrant magnetization can be stabilized by EB. However, to be realizable in practical applications it must be coupled with a larger magnetization to produce a useful flux density. The balance between the volume of FM clusters and compensated host needs to be optimized to combine a large EB with a large magnetization. Hence, the present finding is a good starting point for designing rare-earth-free hard magnets comprising of two hard magnetic phases, which differs from the conventional exchange-spring approach. Our design concept together with the flexibility and huge number of materials crystallizing in the Heusler structure indicate the great potential in designing new materials with a large EB and a large coercivity at room temperature.

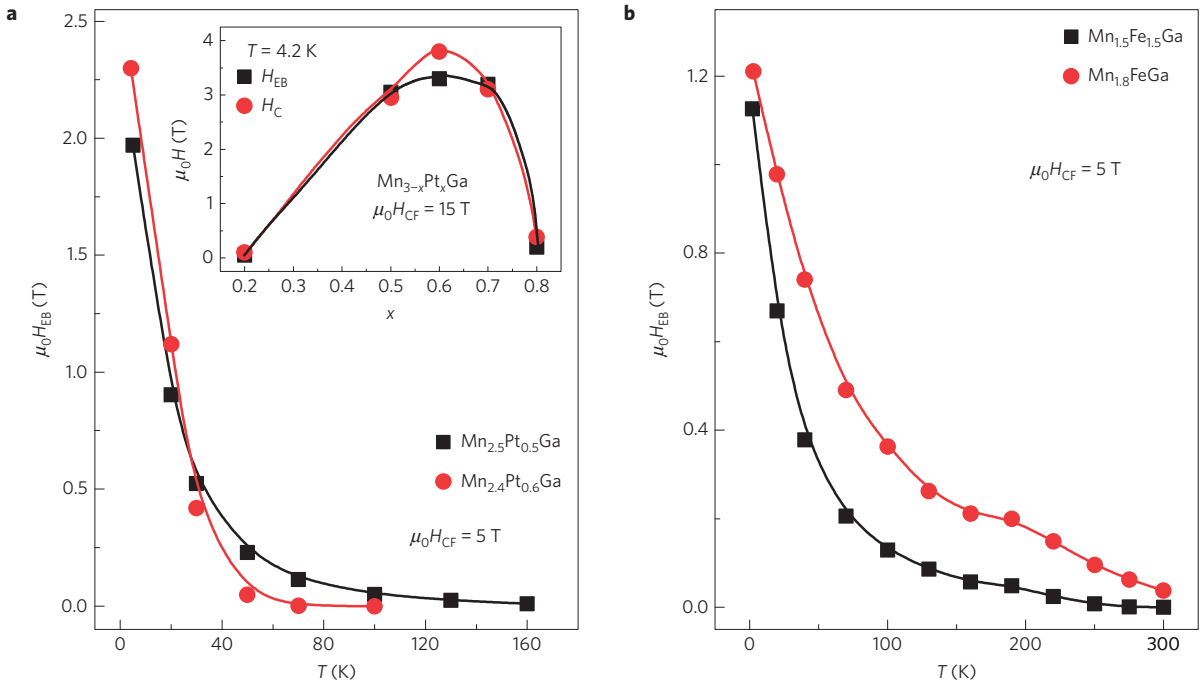

Figure 4 | Exchange bias and coercive fields for Mn–Pt–Ga and Mn–Fe–Ga. a, Temperature dependence of the EB for $Mn_{2.4}Pt_{0.6}Ga$ and $Mn_{2.5}Pt_{0.5}Ga$. The inset shows the coercive field H_C and H_{EB} as a function of the Pt concentration x in $Mn_{3-x}Pt_xGa$. **b**, Temperature dependence of the EB for $Mn_{1.5}Fe_{1.5}Ga$ and $Mn_{1.8}FeGa$. The lines are guides to the eye.

Methods

Polycrystalline ingots of the sample studied in this manuscript were prepared by arc melting stoichiometric amounts of the constituent elements in a high-purity argon atmosphere. The as-prepared ingots were annealed for one week at various temperatures (as mentioned in the Supplementary Information) and subsequently quenched in an ice–water mixture. The samples were structurally characterized by X-ray powder diffraction (XRD) and energy dispersion X-ray analysis (EDAX). The low-field magnetization measurements were performed in different Quantum Design measurement systems in which magnetic fields up to 14 T could be applied. The 32 T static magnetic field measurements were performed using a vibrating-sample-magnetometer at the High Field Magnet Laboratory HFML-RU/FOM in Nijmegen, and the pulsed magnetic field experiments were carried out at the Dresden High Magnetic Field Laboratory HLD-HZDR; both laboratories are members of the European Magnetic Field Laboratory (EMFL). Frequency sweep NMR measurements were carried out using a pulsed Tecmag spectrometer at 4.3 K in zero magnetic field. The spectral intensity was obtained by integrating the spin echo in the time domain recorded at 0.5 MHz after zero-field cooling.

Received 9 July 2014; accepted 9 February 2015;
published online 16 March 2015

References

1. Eberhart, M. E. & Clougherty, D. P. Looking for design in materials design. *Nature Mater.* **3,** 659–661 (2004).
2. Graf, T., Felser, C. & Parkin, S. S. P. Simple rules for the understanding of Heusler compounds. *Prog. Solid State Chem.* **39,** 1–50 (2011).
3. Meiklejohn, W. H. & Bean, C. P. New magnetic anisotropy. *Phys. Rev.* **102,** 1413–1414 (1956).
4. Nogués, J. *et al.* Exchange bias in nanostructures. *Phys. Rep.* **422,** 65–117 (2005).
5. Skumryev, V. *et al.* Beating the superparamagnetic limit with exchange bias. *Nature* **423,** 850–853 (2003).
6. He, X. *et al.* Robust isothermal electric control of exchange bias at room temperature. *Nature Mater.* **9,** 579–585 (2010).
7. Wu, S. M. *et al.* Reversible electric control of exchange bias in a multiferroic field-effect device. *Nature Mater.* **9,** 756–761 (2010).
8. Lage, E. *et al.* Exchange biasing of magnetoelectric composites. *Nature Mater.* **11,** 523–529 (2012).
9. Gider, S., Runge, B. U., Marley, A. C. & Parkin, S. S. P. The magnetic stability of spin-dependent tunneling devices. *Science* **281,** 797–799 (1998).
10. Fernandez-Outon, L. E. *et al.* Large exchange bias IrMn/CoFe for magnetic tunnel junctions. *IEEE Trans. Magn.* **44,** 2824–2827 (2008).
11. Malozemoff, A. P. Random-field model of exchange anisotropy at rough ferromagnetic-antiferromagnetic interfaces. *Phys. Rev. B* **35,** 3679–3682 (1987).
12. Kuch, W. *et al.* Tuning the magnetic coupling across ultrathin antiferromagnetic films by controlling atomic-scale roughness. *Nature Mater.* **5,** 128–133 (2006).
13. Miltènyi, P. *et al.* Diluted antiferromagnets in exchange bias: Proof of the domain state model. *Phys. Rev. Lett.* **84,** 4224–4227 (2000).
14. Nolting, F. *et al.* Direct observation of the alignment of ferromagnetic spins by antiferromagnetic spins. *Nature* **405,** 767–769 (2000).
15. Takano, K., Kodama, R. H., Berkowitz, A. E., Cao, W. & Thomas, G. Interfacial uncompensated antiferromagnetic spins: Role in unidirectional anisotropy in polycrystalline $Ni_{81}Fe_{19}$/CoO bilayers. *Phys. Rev. Lett.* **79,** 1130–1133 (1997).
16. Kodama, R. H., Makhlouf, S. A. & Berkowitz, A. E. Finite size effects in antiferromagnetic NiO nanoparticles. *Phys. Rev. Lett.* **79,** 1393–1396 (1997).
17. Ali, M., Marrows, C. H. & Hickey, B. J. Onset of exchange bias in ultrathin antiferromagnetic layers. *Phys. Rev. B* **67,** 172405 (2003).
18. Wadley, P. *et al.* Tetragonal phase of epitaxial room-temperature antiferromagnet CuMnAs. *Nature Commun.* **4,** 2322 (2013).
19. Soh, Y. & Kummamuru, R. K. Spintronics in antiferromagnets. *Phil. Trans. R. Soc. A* **369,** 3646–3657 (2011).
20. Kimel, A. V., Kirilyuk, A., Tsvetkov, A., Pisarev, R. V. & Rasing, Th. Laser-induced ultrafast spin reorientation in the antiferromagnet $TmFeO_3$. *Nature* **429,** 850–853 (2004).
21. Pickett, W. E. Single spin superconductivity. *Phys. Rev. Lett.* **77,** 3185–3188 (1996).
22. Krenke, T. *et al.* Inverse magnetocaloric effect in ferromagnetic Ni–Mn–Sn alloys. *Nature Mater.* **4,** 450–454 (2005).
23. Kainuma, R. *et al.* Magnetic-field-induced shape recovery by reverse phase transformation. *Nature* **439,** 957–960 (2006).
24. Chadov, S. *et al.* Tunable multifunctional topological insulators in ternary Heusler compounds. *Nature Mater.* **9,** 541–545 (2010).
25. Wurmehl, S., Kandpal, H. C., Fecher, G. H. & Felser, C. Valence electron rules for prediction of half-metallic compensated-ferrimagnetic behaviour of Heusler compounds with complete spin polarization. *J. Phys. Condens. Matter* **18,** 6171–6181 (2006).
26. Chadov, S., Kiss, J. & Felser, C. Improving spin-transport by disorder. *Adv. Funct. Mater.* **23,** 832–838 (2013).
27. Kurt, H. *et al.* Cubic Mn_2Ga thin films: Crossing the spin gap with ruthenium. *Phys. Rev. Lett.* **112,** 027201 (2014).

28. Nayak, A. K. *et al.* Large zero-field cooled exchange-bias in bulk Mn_2PtGa. *Phys. Rev. Lett.* **110,** 127204 (2013).
29. Rode, K. *et al.* Site-specific order and magnetism in tetragonal Mn_3Ga thin films. *Phys. Rev. B* **87,** 184429 (2013).
30. Leighton, C., Nogués, J., Jönsson-Åkerman, B. J. & Schuller, I. K. Coercivity enhancement in exchange biased systems driven by interfacial magnetic frustration. *Phys. Rev. Lett.* **84,** 3466–3469 (2000).

Acknowledgements

We thank J. A. Mydosh and E. Kampert for valuable discussions on the present work. This work was financially supported by the Deutsche Forschungsgemeinschaft DFG (Projects No. TP 1.2-A and No. 2.3-A of Research Unit FOR 1464 ASPIMATT) and by the ERC Advanced Grant No. (291472) 'Idea Heusler'. We acknowledge the support of the High Magnetic Field Laboratory Dresden (HLD) at HZDR and High Field Magnet Laboratory Nijmegen (HFML-RU/FOM), members of the European Magnetic Field Laboratory (EMFL).

Author contributions

All authors contributed substantially to this work.

Additional information

Supplementary information is available in the online version of the paper. Reprints and permissions information is available online at www.nature.com/reprints.
Correspondence and requests for materials should be addressed to A.K.N. or C.F.

Competing financial interests

The authors declare no competing financial interests.